Pyridoclax-loaded nanoemulsion for enhanced anticancer effect on ovarian cancer

A.C. Groo, S. Hedir, M. Since, E. Brotin, L.-B. Weiswald, H. Paysant, G. Nee, M. Coolzaet, D. Goux, R. Delépée, et al.

Research paper

Pyridoclax-loaded nanoemulsion for enhanced anticancer effect on ovarian cancer

A.C. Groo[a*], S. Hedir[b,c], M. Since[a], E. Brotin[b,c,d], L.-B. Weiswald[b,c], H. Paysant[b,c], G. Nee[e], M. Coolzaet[e], D. Goux[f], R. Delépée[g], T. Freret[e], L. Poulain[b,c], A.S. Voisin-Chiret[a], A. Malzert-Fréon[a*]

[a]Normandie Univ, UNICAEN, CERMN, 14000 Caen, France

[b]Normandie Univ, UNICAEN, Inserm U1086 ANTICIPE "Interdisciplinary Research Unit for Cancer Prevention and Treatment", 14000 Caen, France

[c]UNICANCER, Cancer Centre F. Baclesse, 14076 Caen, France

[d]Normandie Univ, UNICAEN, SF4206 Icore, ImpedanCELL Platform, 14000 Caen, France

[e]Normandie Univ, UNICAEN, Inserm U1075, Comete, GIP CYCERON, 14000 Caen, France

[f]Normandie Univ, UNICAEN, CMAbio[3], SF4206 Icore, 14000 Caen, France

[g]Normandie Univ, UNICAEN, PRISMM platform, SF4206 ICORE, Comprehensive Cancer Center F. Baclesse, 14000 Caen, France

*Corresponding authors at: CERMN, UFR des Sciences Pharmaceutiques, Bd Becquerel, 14032 Caen Cedex, France. Tel.: +33231566819.

E-mail addresses: anne-claire.groo@unicaen.fr; aurelie.malzert-freon@unicaen.fr

Keywords: ovarian cancer, nanoemulsions, cytotoxic activity, pharmacokinetics, nanomedicine

ABSTRACT

Background: Pyridoclax is an original lead, recently identified as very promising in treatment of chemoresistant ovarian cancers. To correct the unfavorable intrinsic physico-chemical properties of this BCS II drug, a formulation strategy was implied in the drug discovery step. Pyridoclax-loaded nanoemulsions (NEs) were developed to permit its preclinical evaluation.

Results: The resulting nanoemulsions displayed a mean size of about 100 nm and a high encapsulation efficiency (>95%) at a drug loading of 2 wt%, enabling a 1,000-fold increase of

the Pyridoclax apparent solubility. NEs have enabled a sustained release of the drug as assayed by a dialysis bag method. In addition, anti-tumor effects of the Pyridoclax-loaded nanoemulsions (PNEs) showed a 2.5-fold higher activity on chemoresistant ovarian cancer cells than free Pyridoclax. This effect was confirmed by a drastic increase of caspase 3/7 activation from 10 µM PNEs, as newly objectified by real time apoptose imaging. The Pyridoclax bioavailability was kept unchanged after encapsulation in nanoemulsions as determined in a mice model after oral administration.

Conclusion: Thus, NEs should permit valuable Pyridoclax oral administration, and valorization of this promising anticancer drug by maintaining its original anticancer activity, and by reducing the Pyridoclax therapeutic concentration.

Research paper

Pyridoclax-loaded nanoemulsion for enhanced anticancer effect on ovarian cancer

1. Introduction

Ovarian cancer is the seventh most commonly diagnosed cancer among women in the world, and is responsible of 184,799 deaths worldwide in 2018 (Bray et al., 2018; Momenimovahed et al., 2019; Reid et al., 2017). This common tumor of the reproductive system primarily responds to cytoreductive surgery and cisplatin (DDP)-based chemotherapy (Yang et al., 2019). However, chemoresistance in ovarian cancer results in high mortality (Cornelison et al., 2017). Thus, development of novel strategies to overcome chemoresistance is a central goal in ovarian cancer research (Kim et al., 2018). Pyridoclax is an original drug recently designed by rational drug design approach (Gloaguen et al., 2015). Pyridoclax was identified as the lead compound of an oligopyridine family, acting as a promising protein-protein interactions disruptor. This drug could be particularly interesting in the treatment of ovarian chemoresistant cancers. It is able to induce apoptosis in ovarian cancer cells, when it is administrated in combination with siRNA-mediated Bcl-x_L silencing, or Bcl-x_L targeting molecules such as ABT-737. Indeed, Pyridoclax directly binds to Mcl-1, and hence sensitizes ovarian carcinoma cells to Bcl-x_L targeting strategies. Previously, it has been established that this promising drug appears as a Biopharmaceutics Classification System (BCS) II compound, associated with a good permeability but a low water solubility (Groo et al., 2017). To favor translation for its clinical use, it was essential to improve this drugability parameter. As solubility and permeability are major hindrances to bioavailability, the role of the formulation scientists becomes more and more decisive within the drug development process. Indeed, the formulation strategies are recognized as a really promising method to correct the intrinsic

poor drug-like properties of drug candidates and improve their bioavailability (Ayad, 2015). Chemotherapeutic agents commonly used have various side effects, which include systemic toxicity that reduce the quality of life of patients (Numico et al., 2015; Palesh et al., 2018; Tang et al., 2018). In this aspect, nanoparticle systems have emerged as a new opportunity, since they are able to display a controlled release of their loaded drug, to increase blood circulation time, to decrease the side effects caused by chemotherapeutic agents and to decrease the off-target distribution, or to improve the accumulation of the drug at the targeted tumor site (Ferlay et al., 2019; Raucher et al., 2018; Tang et al., 2018; Tapeinos et al., 2017). On the other hand, their biocompatibility allows them to be easily eliminated or reabsorbed by the patient. In addition, nanomedicine is a promising strategy to deliver anticancer drugs because it could improve cell uptake, increase half-life time in blood and achieve to an accumulation at the tumor site by the Enhanced Permeability and Retention Effect (EPR) (Peer et al., 2007). Thus, the current application of nanoparticle systems has revolutionized cancer treatment by improving the antitumor activity of several chemotherapeutic agents (García-Pinel et al., 2019; Groo et al., 2015).

For this purpose, Pyridoclax-loaded lipid nanoemulsions (PNEs) were efficiently developed and the entrapment in these nanoemulsions has enabled a drastic improvement of its apparent solubility (Groo et al., 2017). The stability of NEPs in biomimetic medium has been also established (Groo et al., 2017). It is now important to determine the biological activity of Pyridoclax after encapsulation, and to evaluate its bioavailability after oral administration of the NEPs.

The aim of this study is to evaluate the impact of encapsulation of Pyridoclax in NEs on its activity against a human chemoresistant ovarian carcinoma cell line *in vitro* and on its pharmacokinetic parameters in mice.

2. Materials and methods

2.1. Materials

$Na_2HPO_4{\cdot}2H_2O$, $Na_2HPO_4{\cdot}H_2O$, $NaH_2PO_4{\cdot}12H_2O$, K_3PO_4, K_2HPO_4, and KH_2PO_4 were obtained from Sigma-Aldrich (Steinheim, Germany). Labrafac® CC (caprylic/capric acid triglycerides) and Labrasol® (caprylocaproyl macrogol-8 glycerides) were kindly provided by Gattefossé S.A. (Saint-Priest, France). Kolliphor® HS15 (70% PEG 660 hydroxystearate and 30% free PEG 660) was a gift from BASF AG (Ludwigshafen, Germany). Methanol, acetonitrile, water of HPLC grade, formic acid, sodium hydroxide, hydrochloric acid were provided by Prolabo VWR International (Fontenay-sous-Bois, France). Sodium chloride was obtained from Carlo Erba (Val de Reuil, France). Pyridoclax was synthesized according to the process previously described (Gloaguen et al., 2015; Voisin-Chiret et al., 2009).

2.2. Methods

2.2.1. Formulation of nanoemulsions

2.2.1.1. Preparation of blank nanoemulsions (NEs) and Pyridoclax-loaded nanoemulsions (PNEs)

The formulation of the nanoemulsion was prepared according to the process previously described (Groo *et al.*, 2017). Briefly, surfactants (Kolliphor® HS15, 30% (w/w), Labrasol®, 50% (w/w), and oil (Labrafac®, 20 % (w/w)) were mixed together and heated under gentle magnetic stirring from room temperature to 85°C, and then cooled down to 25°C. At 25°C, the aqueous phase was suddenly poured into the anhydrous mixture, leading to spontaneous emulsification. The sample was further magnetically stirred (250 rpm) for 30 min at room temperature. To prepare PNEs, 5 mg of Pyridoclax were solubilized in anhydrous mixture. NEs were then formulated as described previously.

2.2.1.2. Characterization of blank and Pyridoclax-loaded nanoemulsions

The average hydrodynamic diameter associated with the polydispersity index (PDI), and the diameter distribution of the nanoemulsions were measured by dynamic light scattering (DLS) using a NanoZS® apparatus (Malvern Instruments SA, Worcestershire, UK). The zeta potential was calculated from the electrophoretic mobility using the Smoluchowski equation. The measurements were performed in triplicate at 25°C, after a 1:100 dilution in distilled water. The morphology of NEs was examined using a transmission electron microscope JEOL 1011 (JEOL, JAPAN) and camera ORIUS 200 (GATAN, FRANCE). Prior to analysis, the NEs were 10-fold diluted with ultrapure water. Then, NEs were dropped on formvar grids previously cleaned by glow discharge (ELMO CORDOUAN Technologies, PESSAC FRANCE). Finally, the sample was shaded with a 1.5 % uranyl acetate solution during fifteen seconds.

To determine the encapsulation efficiency, NEs were filtrated on 0.2 µm regenerated cellulose syringe filters (Fisherbrand, Fisher Scientific, Illkirch, France) in order to eliminate eventual free Pyridoclax. Three samples of filtrate were prepared by dissolution of an exact quantity of PNEs suspension in methanol. Pyridoclax concentrations were then measured by high-performance liquid chromatograph (HPLC). The HPLC method was based on the method previously described (Groo *et al.*, 2017). The mean drug payload (mg/mL of Pyridoclax in NE dispersion) was calculated by comparison to a calibration curve. The encapsulation efficiency (% EE) was calculated by considering the initial amount of drug added in the formulation using Eq. (1):

$$\% \text{ EE} = \frac{\text{Weight of Pyridoclax entrapped within NE}}{\text{Total weight of Pyridoclax added}} \text{x} 100 \quad (1)$$

Drug loading (DL) was calculated using Eq. (2):

$$\% \text{ DL} = \frac{\text{Weight of Pyridoclax entrapped within NE}}{\text{Total weight of oil phase of the NE}} \text{x} 100 \quad (2)$$

Total weight of oil phase of the NE corresponds to the total amount of excipients (excluding the water phase) and Pyridoclax used for the preparation of the NE.

2.2.2. *In vitro* release study

To determine Pyridoclax release profile from nanoemulsions, the dialysis bag method was used. 200 µL of Pyridoclax-NEs was placed into a cellulose ester dialysis tube with 100 kDa pore size (Spectrum lab, CA 90220, USA), and incubated in phosphate buffered saline pH 7.4 (European pharmacopeia, 8th ed.) under gentle horizontal shaking at 37 ± 1°C using a WNB-22 water bath with a SV1422 shaking device (Memmert, Schwabach, Germany). To maintain sink conditions, 1 % (v/v) polysorbate 80 (Tween 80) was added to the acceptor phase. At appropriate intervals, 500 µL samples were withdrawn, assayed, and replaced by fresh buffer. The amount of Pyridoclax in the release medium was determined by HPLC after a 2-fold dilution in methanol. All measurements were performed in triplicate.

2.2.3. *In vitro* activity

2.2.3.1. Cell culture and treatment

The cisplatin-resistant IGROV1-R10 cell line was obtained from IGROV1 cell line as previously described (Villedieu et al., 2007) . Cell line was grown in RPMI-1640 medium supplemented with 2 mM Glutamax™, 25 mM HEPES, 10 % fetal calf serum, and 33 mM sodium bicarbonate (Fisher Scientific Bioblock, France). Cells were maintained in a 5 % CO_2 humidified atmosphere at 37 °C.

ABT-737 was obtained from Selleckchem (Houston, TX, USA) and dimethyl sulfoxide (DMSO) was purchased from Sigma-Aldrich. The compounds were commonly stored as stock solutions in DMSO at −20 °C. For treatment conditions, 24 h after seeding, exponentially growing cells were exposed for 24 h to Pyridoclax as single agent or in combination with ABT-737 at the indicated concentrations.

2.2.3.2. Morphological characterization of apoptotic cells by nuclear staining with DAPI

Both detached and adherent cells were pooled after trypsinisation and applied on a polylysine-coated glass slide by cytospin centrifugation and fixed with a solution of ethanol/chloroform/ acetic acid (6:3:1). The preparations were then incubated with 1 µg/mL DAPI (Boehringer Mannheim, Germany) in water at RT and mounted under a coverslip in Mowiol (Calbiochem, Darmstadt, Germany) and analyzed under a fluorescence microscope (BX51, Olympus, Rungis, France).

2.2.3.3. Cell cycle analysis by flow cytometry

Adherent and floating cells were pooled, washed with 1X PBS and fixed with ethanol 70°. Before flow cytometry analysis, cells were centrifuged at 2000 rpm for 5 min and incubated for 30 min at 37 °C in PBS to allow the release of low-molecular weight DNA (characteristic of apoptotic cells). Cell pellets were stained with propidium iodide (PI) using the DNA Prep Coulter Reagent Kit (Beckman-Coulter, Villepinte France). Samples were thereafter analyzed using a Gallios flow cytometer (Beckman Coulter) and cell cycle distribution was determined using Kaluza acquisition software (Beckman Coulter).

2.2.3.4. IncuCyte apoptosis assay

IGROV1-R10 cells were seeded at 3.5×103 cells in 96-well plates in media. Cells were cultured at 37°C and 5 % CO_2 and monitored using an IncuCyte® S3 (Essen BioScience). IncuCyte® Caspase-3/7 Green Apoptosis Assay Reagent (Essen Bioscience) was added the next day following treatment and baseline images were taken using 10x objective. The plate was scanned and fluorescent and phase-contrast images were acquired in real time every 1 hour from 2 separate regions per well. The Caspase 3/7 reagent labels dead cells yielding green fluorescence. The live-cell phase contrast images were used to calculate confluence

using the IncuCyte® software, and to provide morphology information. Each experiment was done in triplicate and accumulation of caspase 3/7 over time was normalized to confluence of cells.

2.2.4. *In vivo* pharmacokinetic evaluation

2.2.4.1. Animals

NMRI female mice (26–30 g) were provided by Janvier labs (Le Genest-Saint-Isle, France) and kept in our local facility (Centre Universitaire de Ressources Biologiques, Caen, France) under controlled temperature and light conditions (23 ± 2° C, reversed 12h light-dark cycle, light on at 7 pm). *In vivo* experiments started after 15 days of acclimation to the environment. Each animal was gently handled throughout the experiment in accordance with internationally accepted ethical principles for laboratory animal use and care (personal authorization n°14-60), and all efforts were made to minimize animal suffering. This experiment was also carried out in accordance with the 'Good practice guide to the administration of substances and removal of blood, including routes and volumes' adopted by the European Federation of Pharmaceutical Industries Associations (EFPIA) and the European Centre for the Validation of Alternative Methods (ECVAM) in 2001. All experiments were in agreement with the European Directives and French law on animal experimentation, and procedures were approved by national and local ethics committee (Comité d'Ethique Normandie en Matière d'Expérimentation Animale, agreement #2016112413478189).

2.2.4.2. Treatment and sample extraction

Mice were fasted overnight prior to the experiment, but had free access to water. Mice were randomly divided to receive an oral gavage at a dose equivalent to 10 mg/kg of Pyridoclax (200 µL) of either free Pyridoclax suspension (2mg/mL in water with 0.25 % guar gum and 5 % syrup) or Pyridoclax-loaded NEs (2 mg/mL in NaCl 0.09 %). NE formulations were prepared as described above and diluted with NaCl 0.9 % (w/v) to adjust the drug dose for

administration. Blood samples were collected via intracardiac punction into heparinized tubes at 6 different terminal points (20, 60, 90, 120, 240 and 360 minutes) after oral administration (n=3 mice for each time). Plasma samples were separated immediately by centrifugation at 2000 g for 10 minutes. The supernatant plasma fraction was transferred to a clean vial and stored at +4°C for further analysis.

2.2.4.3. Quantification of Pyridoclax in plasma samples

Stock solutions of Pyridoclax and the internal standard, MR29071 (Gloaguen et al., 2015), were prepared in a mixture of ACN and water (80-20, v/v) at 278 and 134 µg/mL respectively and stored at +4 °C.

Calibrators were prepared in plasma (100 µL) by adding 10 µL of ACN containing internal standard (MR29071, 25 µg/mL) and Pyridoclax to yield 0, 50, 100, 250, 500, 1000, 2000, 5000 ng/mL as final concentration followed by vortex agitation and 30 min of incubation at room temperature. Then 400 µL of ACN were added in order to precipitate the proteins and the mixture was centrifuged for 5 min at 13,500 rpm at +4°C. The supernatant was filtered on a 0.2 µm PVDF filter. Then, 100 µL of this solution was diluted with 900 µL of ACN prior to the injection in HPLC-MS/MS system.

Pyridoclax was quantified using an apparatus composed of a NexeraX² HPLC system coupled with LCMS8030Plus (Shimadzu, Kyoto, Japan) mass spectrometer using an electropsray interface in positive mode. The column was a reversed phase column Chromolith RP18e (4.6 x 100 mm) (Merck KGaA, Darmstadt, Germany) maintained at 50 °C. The injection volume and run-to-run time were 50 µL and 10 min, respectively. The flow rate was set to 1 mL/min. Mobile phase was initially composed of a mixture of 60 % water containing 0.05 % (v/v) formic acid and 40 % acetonitrile to reach 100 % in 6 min by applying a linear gradient and

then maintained in this composition for 0.5 min. The composition returned to the initial conditions and the column was equilibrated for 3.5 min.

The mass spectrometer was running in the Multiple Reaction Monitoring (MRM) acquisition mode. LabSolutions 5.86 SP1 software was used to process the data. The desolvatation temperature was 300 °C, source temperature was 400 °C and nitrogen flows were 2.5 L/min for the cone and 15 L/min for the desolvatation. The capillary voltage was +4.5 kV. For each compound, two transitions were followed from the fragmentation of the $[M+H]^+$ ion. The first transition was used for quantification and the second one for confirmation of the compound according to European Commission Decision 2002/657/EC. The transitions used for each compound were summarized in Table 1.

Blank plasma samples were analyzed to check specificity. The calibration curves were drawn by plotting the ratio of the peak high of Pyridoclax to that of the IS. A quadratic regression weighted in 1/C resulted in standard curves with determination coefficients $R^2>0.999$ and more than 75 % of standards with back-calculated concentrations within 15 % of their nominal values as recommended for by the European medicines agency for bioanalytical methods (*EMEA/CHMP/EWP/192217/2009 Rev. 1 Corr. 2**, Guideline on bioanalytical method validation*, 2011). The limits of quantifications for both compounds were considered as the lowest concentrations of the calibration curve.

2.2.4.4. Data analysis

According to the data of plasma drug concentration-time plotted with Graph Pad® Prism statistical software (version 6.01, GraphPad Software, La Jolla, CA, USA) The main pharmacokinetic parameters were calculated, including the area under the plasma drug concentration-time curve ($AUC_{(0\ to\ inf)}$ and $AUC_{(0\ to\ last)}$) calculated using the linear trapezoidal method, the time to reach the maximum plasma drug concentration (T_{max}), the maximum

plasma drug concentration (C_{max}), and the mean transit time (MTT), by non-compartmental analysis using "R" ("R Development Core Team. R: A language and environment for statistical computing. R Foundation for Statistical Computing, Vienna, Austria. ISBN 3-900051-07-0," 2017) software equipped with "PK" package (Jaki and Wolfsegger, n.d.).

3. Results

3.1. Characterization of blank and Pyridoclax-loaded NEs (PNEs)

Unloaded (*i.e.*, blank) and Pyridoclax-loaded NEs were formulated by spontaneous emulsification. Considering that NE formulation permits efficient encapsulation up to a drug loading of 2% of various molecules with very different physico-chemical properties (Gué et al., 2016), we performed Pyridoclax encapsulation assays at 2.0 ± 0.1 wt% drug loading rate. Unloaded and PNEs were characterized in terms of granulometric properties, ζ-potential, and encapsulation efficiency (Table 2).

The mean diameter was 91.0 ± 3.4 nm for blank NEs, and was 105.8 ± 5.1 nm for PNEs. Zeta potential values were neutral for both blank NEs and PNEs. For both formulations, the PDI values were lower than 0.2, indicating narrow size distributions. Encapsulation efficiency of Pyridoclax in NEs at 2.0 wt% drug loading rate (Table 2) was higher than 95%. This corresponds to a drug payload of 4.2 ± 0.3 mg/mL. Such results are in accordance with performances reported previously for the present nanoemulsion formulation (Groo et al., 2017).

Furthermore, transmission electron microscopy (TEM) was employed to evaluate the morphology of the resulting nanoemulsion droplets. TEM study reveals that most of the nanoemulsion droplets containing Pyridoclax were in spherical shape (Figure 1), and diameter measurements were in the same interval than those determined by dynamic light scattering.

3.2. *In vitro* release study

In vitro Pyridoclax release profile has been assessed by using a conventional dialysis bag method. Approximately, half of Pyridoclax loaded in NEs was released in 18 hours into PBS, and up to 87% was released after 96 hours (Figure 2). Release behaviour was fitted according to zero order ($Q = Q_0 + k \times t$), first order ($\ln Q = \ln Q_0 + k \times t$), and square root of time ($Q = k \times \sqrt{t}$) models) models, where Q (mg) denotes the cumulative amount of drug released at time t (h), Q_0 is the initial amount of drug at t = 0, and k is the release constant. Regression coefficient and drug release rate constants obtained from slopes are shown in Table 3. Considering the linear relationship between the cumulative amount of drug released and √t that was obtained, it appears that the release profile of Pyridoclax best fit into a square root of time model. It can be noted that the Higuchi equation, describing diffusional release from a thin film, would be misused in the present study since various defining conditions are violated (Siepmann and Peppas, 2011).

3.3. *In vitro* activity

3.3.1. Effect of Pyridoclax on ovarian carcinoma cell line IGROV1-R10

Considering that ABT-737 is one of the most potent Bcl-x_L inhibiting BH3-mimetic molecules and because the response of ovarian cancer IGROV1-R10 cells to ABT-737 is conditioned by the inhibition of Mcl-1, we evaluated the effect of the combination of ABT-737 with Pyridoclax (Figure 3). Neither 24 h of Pyridoclax treatment alone nor ABT-737 alone induced massive cell death on their own. We observed a slowed cell proliferation, but neither cell detachment, strong sub-G1 peak, nor condensed or fragmented nuclei that constitute apoptotic features, were detected in these conditions (Figure 3).

In contrast, the combination of Pyridoclax with ABT-737 led to massive cell death, as demonstrated by drastic cell detachment, and by the appearance of a strong sub-G1 peak on the DNA content histogram (up to 50%) (Figure 3). DAPI staining and phase contrast microscopy showed that this combination induced nuclear condensations and fragmentations,

that are highly evocative of apoptotic cell death (Figure 3). We showed that these effects were optimal after exposure to 25 µM of Pyridoclax but were also observed to a lower extent in response to 10 µM (Figure 3).

3.3.2. Effect of blanks NEs and Pyridoclax-loaded NEs (PNEs) on ovarian carcinoma cell line IGROV1-R10

Neither unloaded NEs nor Pyridoclax-loaded NEs (PNEs) induced cell death as single agents (Figure 3). On the contrary, the combination of PNEs with ABT-737 led to massive apoptotic cell death in IGROV1-R10 chemoresistant ovarian cancer cell line, correlated with a strong cell detachment, and with the appearance of a strong sub-G1 peak on the DNA content histogram (over 60 %) (Figure 3). DAPI staining and phase contrast microscopy showed that this combination led to nuclear condensations and fragmentations highly evocative of apoptotic cell death (Figure 3). Encapsulated within the NE, Pyridoclax becomes strongly active at the concentration of 10 µM, *vs* 25 µM for the unloaded drug. The use of NEs thus potentiate Pyridoclax activity, and allow a 2.5-fold decrease of the therapeutic concentration of Pyridoclax when used in association with ABT-737. A higher PNEs concentration (25 µM) with ABT-737 induced a drastic cell detachment and a massive cell death on IGROV1-R10 cells (Figure 3).

The Figure 4 confirmed that neither ABT-737 nor Pyridoclax induced a caspase 3/7 activity, as assessed by real time cell imaging. The combination of ABT-737 with Pyridoclax led to a cell death at 25 µM of Pyridoclax (Figure 4), as expected. Neither blanks NEs nor PNEs alone induced caspase 3/7 activity (Figure 4) whereas the combination of ABT-737 and Pyridoclax-loaded NEs induced a higher and faster caspase 3/7 activation (Figure 4) at 10 µM than the combination of ABT and free Pyridoclax at 25 µM.

3.4. *In vivo* pharmacokinetics evaluation

Plasma concentration *vs* time profiles of Pyridoclax after oral administration of Pyridoclax suspension or PNEs are presented in Figure 5. Pharmacokinetic parameters of non-compartmental analysis (C_{max}, T_{max}, AUC and Mean Transit Time (MTT)) are given in Table 4. When Pyridoclax was loaded NEs, its profile was not significantly different from that of Pyridoclax suspension (figure 5). The C_{max} was 1200 ± 751 for PNEs, and was 1330 ± 609 ng/ml for Pyridoclax suspension. Similarly, after oral administration of PNEs, the $AUC_{(0\ to\ inf)}$, $AUC_{(0\ to\ last)}$ and the MTT were not different from that of Pyridoclax suspension. T_{max} was decreased from 60 to 20 min when Pyridoclax was loaded in NEs.

4. Discussion

Pyridoclax was identified as the lead compound of an oligopyridine family that could be efficiently used as a Mcl-1 inhibitor, particularly of interest in ovarian cancer treatment (Gloaguen et al., 2015). However, from results of previous studies performed in our team, Pyridoclax appears as a BCS II drug (Groo et al., 2017).

More generally, the widespread use of modern discovery tools such as high throughput screening and rational drug design approaches have contributed to the emergence of lead candidates with higher molecular weight and/or increased lipophilicity. As such properties directly and negatively impact aqueous solubility and permeability of molecules, they can also limit their oral absorption, and *in fine* their bioavailability. Performing of efficient preclinical studies on such lead molecules may be challenging. Indeed, it is crucial to achieve an acceptable and reproducible exposure for pharmacology and/or toxicology studies (Li and Zhao, 2007). Pharmacokinetics experiments are also necessary to characterize molecules during drug discovery (Neervannan, 2006).

To correct the unfavorable intrinsic physico-chemical properties of such leads, and to enable preclinical studies with accurate dosing, optimum exposure at the target site, and minimized

toxic side effects by appropriate choice of solvents and excipients, different formulation strategies can be proposed from preclinical studies (Ayad, 2015; Chen et al., 2012).

The Revised General Solubility Equation (GSE), in particular after rearrangement, can be helpful to define the limiting factor for drug solubility, and hence, the best formulation strategy to use (Ayad, 2015; Ran et al., 2001) : LogSw = 0.75 – (logP + Mp/100).

If the log of the *n*-octanol-water partition coefficient (*i.e.*, logP) is lower than the melting point MP/100, the poor solubility of the molecule could be increased by reducing the high crystal lattice forces within the molecule, for example, by producing solid dispersions or nano-crystals.

Considering the calculated log of the *n*-octanol-water partition coefficient (*i.e.*, calc logP=5.8) or the lipophilicity experimentally determined by chromatographic method (*i.e.*, chrom logP=4.4), and the melting point (*i.e.*, mp=158°C) of Pyridoclax (De Pascale et al., 2020), logP appears higher than mp/100. From that, the solubility of Pyridoclax being rather logP limited, the challenging molecule appears as a good candidate for formulation of Self Emulsifying Drug Delivery Systems (SEDDS) (Ayad, 2015), or nanoemulsions as those that we have recently developed (Groo et al., 2017; Gué et al., 2016).

Pyridoclax was incorporated in NEs with a high encapsulation efficiency (> 95%) at a drug loading of 2 wt%. No effect of the drug on the size distribution of NEs was observed in comparison with the unloaded NEs, since a monodisperse population is obtained in both cases. The size of NEs slightly increased in presence of Pyridoclax. Considering the unionized state of the drug in the conditions of the experiments, it is coherent to keep a neutral zeta potential value after Pyridoclax incorporation. These results are in accordance with previous studies, in particular, with those reported for ibuprofen, another BCS class II compound. Indeed, it was showed that its incorporation in the formulation leads to high drug recovery and droplet size increase, all the more important as the active pharmaceutical ingredient (API)

loading rate increases. It was suggested that ibuprofen molecules were encapsulated into the oily core due to the hydrophobic character of the drug, but that some ibuprofen molecules participate also to oil–water interfaces, within Labrasol® and Kolliphor® HS15 molecules, resulting in nanoemulsions with larger droplet sizes (Groo et al., 2017).

PNEs stability has been previously studied in PBS at 37°C, and no drug release was observed for 3 h (Groo et al., 2017). However, from results of the present *in vitro* release kinetics study assessed by the conventional dialysis bag method, it appeared that 19 % of Pyridoclax was released from PNEs after 3 h. With such a method, sink conditions must be maintained. In this goal, 1 % (v/v) polysorbate 80 (Tween® 80) was added in PBS whereas in the previous stability study, PBS without polysorbate 80 was used as biomimetic medium. This medium change could explain the difference in the kinetics release profile. Gué *et al* explored the formulate-ability of six model active pharmaceutical ingredients (API), with different physico-chemical profiles, in the NEs and studied their release in similar maintained sink conditions (Gué et al., 2016). Among these API, fenofibrate presents log P and log D values (5.3 and 5.28, respectively) in the same magnitude order than those of Pyridoclax (5.68 and 5.27, respectively). Sustained release of 59% of fenofibrate in 22 days was observed for fenofibrate-loaded NEs whereas 58% of Pyridoclax was released in 18 hours. The Pyridoclax release appears faster, maybe due to the difference of solubility of the compounds at pH 7.4 (0.8 µM for fenofibrate *vs* 9.4 µM for Pyridoclax). Complete, sustained but rather rapid release of ibuprofen was reached in 8 h. However, for all drugs, a linear relationship between the cumulative amount of drug released and √t is obtained. Drug release rate constant K ($mg.h^{-1/2}$) of Pyridoclax according to this relationship was five-fold higher than that of fenofibrate and three-fold lower than that of ibuprofen. Pyridoclax loading decreases droplet size. This phenomenon was observed previously when ibuprofen was encapsulated in NEs. It was suggested that ibuprofen and Pyridoclax molecules were encapsulated into the oily core,

but that some molecules participate also to oil–water interfaces, resulting to a more rapid release than for fenofibrate. However, the proportion of Pyridoclax molecules at the interface could be lower than that of ibuprofen considering the ibuprofen log P, log D and values (4.13 and 0.45, respectively) and could explain the slower release.

The IGROV1-R10 human ovarian cancer cell line is addicted to both Bcl-x_L and Mcl-1 for its survival (Villedieu et al., 2007). This feature can be easily used for the screening of anti-apoptotic pharmacological inhibitors of Bcl-2 family anti-apoptotic proteins (Gloaguen et al., 2015). Indeed, its pharmacological inhibition by ABT-737 does not induce cell death on its own but strongly sensitizes cells to Mcl-1 inhibition. The resistant IGROV1-R10 ovarian cancer cells were treated by Pyridoclax or NEPs, alone or in combination with ABT-737. In accordance with a previous study, unencapsulated Pyridoclax is able to induce strong cell apoptosis when it is used in combination with ABT-737, from the concentration of 10 µM, and is the most strongly active at 25 µM (Figure 3). All the biological observations showed that the activity of PNEs at 10 µM, when combined with ABT-737, become similar to Pyridoclax at 25 µM, whereas no toxicity of the NEs is observed on their own (Figure 3). Thus, encapsulation of Pyridoclax into NEs permits to potentiate its activity, and to obtain a 2.5-fold decrease of the therapeutic concentration of Pyridoclax when used in association with ABT-737. The combination of ABT-737 and 10 µM PNEs induced a high caspase 3/7 activation (Figure 4), correlated to a massive cell death.

As determined from the release kinetics studies (Figure 2), only 28 % of Pyridoclax are released after 5 hours in PBS at 37°C. Effect of PNEs, used in combination with ABT-737, was objectified from the first 5 hours on caspase 3-7 activity assessed by real time IGROV1-R10 cells imaging (Figure 4). Thus, PNEs treatment effect can be attributed to Pyridoclax loaded into NEs and not to a release of Pyridoclax from NEs. The improvement of Pyridoclax activity when it is encapsulated in NEs could be attributed to the enhanced cell uptake.

Nanocarriers are well known to increase the drug cell uptake, by promoting the endocytosis (Behzadi et al., 2017). When nanocarriers reach the extern membrane of a cell, they can interact with membrane components or extracellular matrix and enter into the cell, mainly through endocytosis. The successful cellular uptake means that the nanoemulsion formulation can deliver its payload more efficiently than the drug solution (Sánchez-López et al., 2019). In the study of Liu *et al.*, the encapsulation of evodiamine in nanoemulsions enabled an efficient intracellular delivery by endocytosis, leading to a higher cytotoxicity on A549 cells (Liu et al., 2017). Similarly Guan *et al.* have shown that the cytotoxicity, cell uptake, cell cycle arrest and apoptosis were considerably increased with curcumine-loaded nanoemulsions compared to free curcumine, on prostate cancer cells (Guan et al., 2017).

Chemotherapy is usually administered by intravenous injection, but inclination towards oral administration of anticancer drug is increasing since it offers better quality of life, treatment advantages and low healthcare cost (Thanki et al., 2013). However, optimization of oral treatment with maximized efficacy and minimal side effects is a challenge (Tariq et al., 2016). Oral delivery is very convenient but can be very difficult for drugs belonging to class II of the biopharmaceutical classification system, such as Pyridoclax.

In the past few years, the growth of nanometric size drug delivery systems (DDS) has permitted real progresses to achieve oral delivery of anticancer drugs (Mazzaferro et al., 2013). Drug encapsulation into nanomedicine has allowed to improved bioavailability and drug efficacy (Cui et al., 2019; Ezzat et al., 2019; Groo et al., 2015; Youssef et al., 2018). Moreover, hydrophobic drugs encapsulation would facilitate drug transition from carrier to a cell (Teymouri et al., 2019) and presents an real interest for Pyridoclax delivery.

PNEs were administrated orally to mice and parameters were compared to that of Pyridoclax. In order to not modify Pyridoclax pharmacokinetics and administer a controlled concentration, drug suspension was chosen as formulation for free Pyridoclax. Indeed,

aqueous solution formulation was not possible due to the lipophilic character of Pyridoclax. The use of surfactants is well-known to possibly modify pharmacokinetics profiles, and, for this reason, micellar formulation was avoided. From results, it appeared that encapsulation of Pyridoclax into NEs did not improve its bioavailability (Figure 5 and Table 4). $C_{max,}$ AUC and MTT were similar to values determined for Pyridoclax used under oral suspension (Table 4). So, despite a good solubilisation into NEs, vectorization strategy to improve the bioavailability of Pyridoclax was not objectified.

For some compounds, the relation between poor solubility and poor bioavailability appears as not true. Indeed, satisfying absorption of a poorly soluble drug can be achieved thanks to compensatory mechanisms between solubility and permeability in the intestine (Kostewicz et al., 2014). After oral administration, the concentration of a drug in the small intestine may be calculated to exceed its intrinsic solubility. Nevertheless, if the drug has a high permeability, sink conditions permit further dissolution of the molecule, and it is kept into solution. In this case, the absorption of the compound is only limited by its dissolution ability. On the opposite, if the permeability of the drug is low, no compensatory mechanisms further permit dissolution of the compound and its absorption remains limited by its solubility.

To make the distinction between both types of molecules, the Developability Classification System (DCS), and more recently its refined version (rDSC), was proposed by Dressman and her co-workers (Butler and Dressman, 2010; Rosenberger et al., 2018). This classification keeps unchanged classes I, III, and IV of the Biopharmaceutics Classification System (BCS) introduced by Amidon *et al*. in the 1990s, and initially developed for regulatory assess the possibility of bioequivalence of drugs based on their aqueous solubility and intestinal permeability (Amidon et al., 1995). However, the class II becomes divided into 2 subclasses a, and b, as the absorption of compounds is limited or by their dissolution, or by their solubility, respectively (Butler and Dressman, 2010).

Although being poorly soluble, Pyridoclax presents a good permeability (Pe = 160 nm/s) as previously determined from gastrointestinal- parallel artificial membrane permeability assay (GIT-PAMPA assay) (De Pascale et al., 2020; Groo et al., 2017). This method is well adapted for HTS, and during the early stages of drug discovery (Kansy et al., 1998), where it is considered sufficient to evaluate compounds with regard to high or low permeability (Avdeef et al., 2007). From that, Pyridoclax could behave as a rDSC class IIa compound.

Moreover, according to the DSC recommendations, drug solubility should be determined in fasted state simulated intestinal fluid (FaSSIF) rather than in simple buffer to more accurately predict *in vivo* API performance (Butler and Dressman, 2010). Solubility of a Pyridoclax salt was previously determined to be about 8 µg/mL in FaSSIF-V2. It has been also established that this compound remained well solubilized in time in this medium. It was better solubilized in high presence of lipids and surfactants, as in fed state simulating intestinal fluid (FeSSIF-V2), which could help to solubilize the drug by formation of micelles (Groo et al., 2017).

Thus, the presence of lipids all along the gastrointestinal tract could improve the solubilisation of Pyridoclax after oral administration, and *in fine*, contribute also to satisfactory bioavailability.

Differences of MTT have been shown between free Pyridoclax and Pyridoclax-loaded nanoemulsions. Lymphatic drug transport has been reported to be a contributor in the oral bioavailability in various lipophilic drugs and xenobiotics after oral administration (Yáñez et al., 2011). It is known in particular that highly lipophilic (*i.e.*, log P > 5) compounds are likely to be involved in intestinal lymphatic transport. For lipid based-delivery systems, the intestinal lymphatic transport appears dependent on the nature of lipid excipients. Medium-chain fatty acids, as the glycerides used in our formulation, would be more readily absorbed by the portal blood than long-chain fatty acids. At this stage, it is not possible to further explain observed differences in MTT. Nevertheless, from PK results, it appears that, if it is

encapsulated in nanoemulsions, Pyridoclax is well absorbed after oral administration, and its biodistribution through the blood circulation becomes modified thanks to the use of the delivery system.

Pyridoclax encapsulation into NEs leads to an enhanced *in vitro* effect on resistant ovarian cancer cell in combination with ABT-737, and maintains the bioavailability after oral administration to mice. Considering these first crucial results, it seems interesting to further determine if NEs improve *in vivo* activity of Pyridoclax, and if the use of a reduced therapeutic concentration is enabled as suggested by the biological *in vitro* studies. Although Pyridoclax has a sufficient bioavailability, the vectorization could modify biodistribution with an accumulation in tumor site and improve cell uptake. These phenomena may contribute to enhance the anticancer activity of this promising drug, not only thanks to a reduced dose but also by permitting passive targeting *via* EPR effect thanks to the composition of the developed NE.

5. Conclusion

This study is the first evaluation of PNEs as treatment against resistant ovarian cancer cells. Encapsulation of Pyridoclax in NEs enhanced its activity on ovarian cancer cells *in vitro* and allowed a 2.5-fold reduction of its therapeutic concentration. Oral ingestion of drugs is considered as the most accepted and preferred mode of drug administration. In order to envisage oral chemotherapy, PNE bioavailability was evaluated after oral administration in mice model. Encapsulation into NEs did not improve the Pyridoclax bioavailability. However, nanocarriers are well-known to modify biodistribution. Particularly, nanocarriers of anticancer drug could allow to improve tumor accumulation of drug.

Declaration of Interest

The authors declare no completing financial of interest.

Acknowledgements

This work was financially supported by the Cancéropôle Nord-Ouest (canceropole-nordouest.org). This work was also financially supported by the Region Normandie and the European Union *via* the European Regional Development Fund (FEDER).

No writing assistance was utilized in the production of this manuscript.

References

Amidon, G.L., Lennernäs, H., Shah, V.P., Crison, J.R., 1995. A theoretical basis for a biopharmaceutic drug classification: the correlation of in vitro drug product dissolution and in vivo bioavailability. Pharmaceutical research 12, 413–20.

Avdeef, A., Bendels, S., Di, L. i., Faller, B., Kansy, M., Sugano, K., Yamauchi, Y., 2007. PAMPA—critical factors for better predictions of absorption. Journal of Pharmaceutical Sciences 96, 2893–2909. https://doi.org/10.1002/JPS.21068

Ayad, M.H., 2015. Rational formulation strategy from drug discovery profiling to human proof of concept. Drug Delivery 22, 877–884. https://doi.org/10.3109/10717544.2014.898714

Behzadi, S., Serpooshan, V., Tao, W., Hamaly, M.A., Alkawareek, M.Y., Dreaden, E.C., Brown, D., Alkilany, A.M., Farokhzad, O.C., Mahmoudi, M., 2017. Cellular uptake of nanoparticles: journey inside the cell. Chem. Soc. Rev. 46, 4218–4244. https://doi.org/10.1039/C6CS00636A

Bray, F., Ferlay, J., Soerjomataram, I., Siegel, R.L., Torre, L.A., Jemal, A., 2018. Global cancer statistics 2018: GLOBOCAN estimates of incidence and mortality worldwide for 36 cancers in 185 countries. CA: A Cancer Journal for Clinicians 68, 394–424. https://doi.org/10.3322/caac.21492

Butler, J.M., Dressman, J.B., 2010. The Developability Classification System: Application of Biopharmaceutics Concepts to Formulation Development. Journal of Pharmaceutical Sciences 99, 4940–4954. https://doi.org/10.1002/JPS.22217

Chen, X.Q., Gudmundsson, O.S., Hageman, M.J., 2012. Application of lipid-based formulations in drug discovery. Journal of Medicinal Chemistry 55, 7945–7956. https://doi.org/10.1021/jm3006433

Cornelison, R., Llaneza, D.C., Landen, C.N., 2017. Emerging Therapeutics to Overcome Chemoresistance in Epithelial Ovarian Cancer: A Mini-Review. Int J Mol Sci 18, 2171. https://doi.org/10.3390/ijms18102171

Cui, W., Zhao, H., Wang, C., Chen, Y., Luo, C., Zhang, S., Sun, B., He, Z., 2019. Co-encapsulation of docetaxel and cyclosporin A into SNEDDS to promote oral cancer chemotherapy. Drug Deliv 26, 542–550. https://doi.org/10.1080/10717544.2019.1616237

De Pascale, M., Iacopetta, D., Since, M., Corvaisier, S., Vie, V., Paboeuf, G., Hennequin, D., Perato, S., De Giorgi, M., Sinicropi, M.S., Sopkova-De Oliveira Santos, J., Voisin-Chiret, A.-S., Malzert-Freon, A., 2020. Synthesis of Pyridoclax Analogues: Insight into Their Druggability by Investigating Their Physicochemical Properties and Interactions with Membranes. ChemMedChem 15, 136–154. https://doi.org/10.1002/cmdc.201900542

EMEA/CHMP/EWP/192217/2009 Rev. 1 Corr. 2**, Guideline on bioanalytical method validation, 2011.

Ezzat, H.M., Elnaggar, Y.S.R., Abdallah, O.Y., 2019. Improved oral bioavailability of the anticancer drug catechin using chitosomes: Design, in-vitro appraisal and in-vivo studies. Int J Pharm 565, 488–498. https://doi.org/10.1016/j.ijpharm.2019.05.034

Ferlay, J., Colombet, M., Soerjomataram, I., Mathers, C., Parkin, D.M., Piñeros, M., Znaor, A., Bray, F., 2019. Estimating the global cancer incidence and mortality in 2018: GLOBOCAN sources and methods. International Journal of Cancer 144, 1941–1953. https://doi.org/10.1002/ijc.31937

García-Pinel, B., Porras-Alcalá, C., Ortega-Rodríguez, A., Sarabia, F., Prados, J., Melguizo, C., López-Romero, J.M., 2019. Lipid-Based Nanoparticles: Application and Recent Advances in Cancer Treatment. Nanomaterials (Basel) 9. https://doi.org/10.3390/nano9040638

Gloaguen, C., Voisin-Chiret, A.S., Sopkova-De Oliveira Santos, J., Fogha, J., Gautier, F., De Giorgi, M., Burzicki, G., Perato, S., Pétigny-Lechartier, C., Simonin-Le Jeune, K., Brotin, E., Goux, D., N'Diaye, M., Lambert, B., Louis, M.H., Ligat, L., Lopez, F., Juin, P., Bureau, R., Rault, S., Poulain, L., 2015. First evidence that oligopyridines, α-helix foldamers, inhibit Mcl-1 and sensitize ovarian carcinoma cells to Bcl-x<inf>L</inf>-targeting strategies. Journal of Medicinal Chemistry 58, 1644–1668. https://doi.org/10.1021/jm500672y

Groo, A.C., Bossiere, M., Trichard, L., Legras, P., Benoit, J.P., Lagarce, F., 2015. In vivo evaluation of paclitaxel-loaded lipid nanocapsules after intravenous and oral administration on resistant tumor. Nanomedicine (Lond) 10, 589–601. https://doi.org/10.2217/nnm.14.124

Groo, A.-C., De Pascale, M., Voisin-Chiret, A.-S., Corvaisier, S., Since, M., Malzert-Fréon, A., 2017. Comparison of 2 strategies to enhance pyridoclax solubility: Nanoemulsion delivery system versus salt synthesis. European Journal of Pharmaceutical Sciences 97, 218–226. https://doi.org/10.1016/j.ejps.2016.11.025

Guan, Y.-B., Zhou, S.-Y., Zhang, Y.-Q., Wang, J., Tian, Y.-D., Jia, Y.-Y., Sun, Y.-J., 2017. Therapeutic effects of curcumin nanoemulsions on prostate cancer. J. Huazhong Univ. Sci. Technol. Med. Sci. 37, 371–378. https://doi.org/10.1007/s11596-017-1742-8

Gué, E., Since, M., Ropars, S., Herbinet, R., Le Pluart, L., Malzert-Fréon, A., 2016. Evaluation of the versatile character of a nanoemulsion formulation. International Journal of Pharmaceutics 498, 49–65. https://doi.org/10.1016/j.ijpharm.2015.12.010

Jaki, T., Wolfsegger, M.J., n.d. PK: Basic Non-Compartmental Pharmacokinetics., in: R Package Version 1.3-4.

Kansy, M., Senner, F., Gubernator, K., 1998. Physicochemical high throughput screening: Parallel artificial membrane permeation assay in the description of passive absorption processes. Journal of Medicinal Chemistry 41, 1007–1010. https://doi.org/10.1021/jm970530e

Kim, S., Han, Y., Kim, S.I., Kim, H.-S., Kim, S.J., Song, Y.S., 2018. Tumor evolution and chemoresistance in ovarian cancer. NPJ Precis Oncol 2. https://doi.org/10.1038/s41698-018-0063-0

Kostewicz, E.S., Abrahamsson, B., Brewster, M., Brouwers, J., Butler, J., Carlert, S., Dickinson, P.A., Dressman, J., Holm, R., Klein, S., Mann, J., McAllister, M., Minekus, M., Muenster, U., Müllertz, A., Verwei, M., Vertzoni, M., Weitschies, W., Augustijns, P., 2014. In vitro models for the prediction of in vivo performance of oral dosage forms. European Journal of Pharmaceutical Sciences 57, 342–366. https://doi.org/10.1016/j.ejps.2013.08.024

Li, P., Zhao, L., 2007. Developing early formulations: Practice and perspective. International Journal of Pharmaceutics 341, 1–19. https://doi.org/10.1016/J.IJPHARM.2007.05.049

Liu, S., Chen, D., Yuan, Y., Zhang, X., Li, Y., Yan, S., Zhang, J., 2017. Efficient intracellular delivery makes cancer cells sensitive to nanoemulsive chemodrugs. Oncotarget 8, 65042–65055. https://doi.org/10.18632/oncotarget.17536

Mazzaferro, S., Bouchemal, K., Ponchel, G., 2013. Oral delivery of anticancer drugs III: formulation using drug delivery systems. Drug Discovery Today 18, 99–104. https://doi.org/10.1016/j.drudis.2012.08.007

Momenimovahed, Z., Tiznobaik, A., Taheri, S., Salehiniya, H., 2019. Ovarian cancer in the world: epidemiology and risk factors. Int J Womens Health 11, 287–299. https://doi.org/10.2147/IJWH.S197604

Neervannan, S., 2006. Preclinical formulations for discovery and toxicology: physicochemical challenges. Expert Opinion on Drug Metabolism & Toxicology 2, 715–731. https://doi.org/10.1517/17425255.2.5.715

Numico, G., Longo, V., Courthod, G., Silvestris, N., 2015. Cancer survivorship: long-term side-effects of anticancer treatments of gastrointestinal cancer. Current Opinion in Oncology 27, 351–357. https://doi.org/10.1097/CCO.0000000000000203

Palesh, O., Scheiber, C., Kesler, S., Mustian, K., Koopman, C., Schapira, L., 2018. Management of side effects during and post-treatment in breast cancer survivors. The Breast Journal 24, 167–175. https://doi.org/10.1111/tbj.12862

Peer, D., Karp, J.M., Hong, S., Farokhzad, O.C., Margalit, R., Langer, R., 2007. Nanocarriers as an emerging platform for cancer therapy. Nature Nanotechnology 2, 751–760. https://doi.org/10.1038/nnano.2007.387

R Development Core Team. R: A language and environment for statistical computing. R Foundation for Statistical Computing, Vienna, Austria. ISBN 3-900051-07-0 [WWW Document], 2017. URL http://www.R-project.org

Ran, Y., Jain, N., Yalkowsky, S.H., 2001. Prediction of Aqueous Solubility of Organic Compounds by the General Solubility Equation (GSE). Journal of Chemical Information and Computer Sciences 41, 1208–1217. https://doi.org/10.1021/ci010287z

Raucher, D., Dragojevic, S., Ryu, J., 2018. Macromolecular Drug Carriers for Targeted Glioblastoma Therapy: Preclinical Studies, Challenges, and Future Perspectives. Front. Oncol. 8. https://doi.org/10.3389/fonc.2018.00624

Reid, B.M., Permuth, J.B., Sellers, T.A., 2017. Epidemiology of ovarian cancer: a review. Cancer Biol Med 14, 9–32. https://doi.org/10.20892/j.issn.2095-3941.2016.0084

Rosenberger, J., Butler, J., Dressman, J., 2018. A Refined Developability Classification System. Journal of Pharmaceutical Sciences 107, 2020–2032. https://doi.org/10.1016/j.xphs.2018.03.030

Sánchez-López, E., Guerra, M., Dias-Ferreira, J., Lopez-Machado, A., Ettcheto, M., Cano, A., Espina, M., Camins, A., Garcia, M.L., Souto, E.B., 2019. Current Applications of

Nanoemulsions in Cancer Therapeutics. Nanomaterials (Basel) 9. https://doi.org/10.3390/nano9060821
Siepmann, J., Peppas, N.A., 2011. Higuchi equation: derivation, applications, use and misuse. Int J Pharm 418, 6–12. https://doi.org/10.1016/j.ijpharm.2011.03.051
Tang, W.-L., Tang, W.-H., Li, S.-D., 2018. Cancer theranostic applications of lipid-based nanoparticles. Drug Discovery Today 23, 1159–1166. https://doi.org/10.1016/j.drudis.2018.04.007
Tapeinos, C., Battaglini, M., Ciofani, G., 2017. Advances in the design of solid lipid nanoparticles and nanostructured lipid carriers for targeting brain diseases. Journal of Controlled Release 264, 306–332. https://doi.org/10.1016/j.jconrel.2017.08.033
Tariq, M., Singh, A.T., Iqbal, Z., Ahmad, F.J., Talegaonkar, S., 2016. Investigative Approaches for Oral Delivery of Anticancer Drugs: A Patent Review. Recent Pat Drug Deliv Formul 10, 24–43.
Teymouri, M., Mashreghi, M., Saburi, E., Hejazi, A., Nikpoor, A.R., 2019. The trip of a drug inside the body: From a lipid-based nanocarrier to a target cell. Journal of Controlled Release 309, 59–71. https://doi.org/10.1016/j.jconrel.2019.07.027
Thanki, K., Gangwal, R.P., Sangamwar, A.T., Jain, S., 2013. Oral delivery of anticancer drugs: challenges and opportunities. J Control Release 170, 15–40. https://doi.org/10.1016/j.jconrel.2013.04.020
Villedieu, M., Louis, M.-H., Dutoit, S., Brotin, E., Lincet, H., Duigou, F., Staedel, C., Gauduchon, P., Poulain, L., 2007. Absence of Bcl-xL down-regulation in response to cisplatin is associated with chemoresistance in ovarian carcinoma cells. Gynecol. Oncol. 105, 31–44. https://doi.org/10.1016/j.ygyno.2006.12.011
Voisin-Chiret, A.S., Bouillon, A., Burzicki, G., Célant, M., Legay, R., El-Kashef, H., Rault, S., 2009. A general synthesis of halo-oligopyridines. The Garlanding concept. Tetrahedron 65, 607–612. https://doi.org/10.1016/j.tet.2008.11.024
Yáñez, J.A., Wang, S.W.J., Knemeyer, I.W., Wirth, M.A., Alton, K.B., 2011. Intestinal lymphatic transport for drug delivery. Advanced Drug Delivery Reviews 63, 923–942. https://doi.org/10.1016/j.addr.2011.05.019
Yang, C., Zhao, N., Li, D., Zou, G., Chen, Y., 2019. Metformin improves the sensitivity of ovarian cancer cells to chemotherapeutic agents. Oncol Lett 18, 2404–2411. https://doi.org/10.3892/ol.2019.10564
Youssef, S.F., Elnaggar, Y.S., Abdallah, O.Y., 2018. Elaboration of polymersomes versus conventional liposomes for improving oral bioavailability of the anticancer flutamide. Nanomedicine (Lond) 13, 3025–3036. https://doi.org/10.2217/nnm-2018-0238

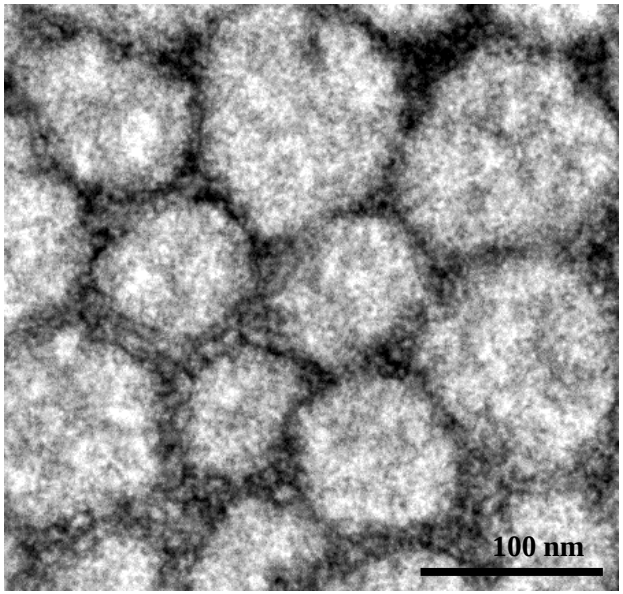

Figure 1. Transmission electron microscopy (TEM) of PNEs

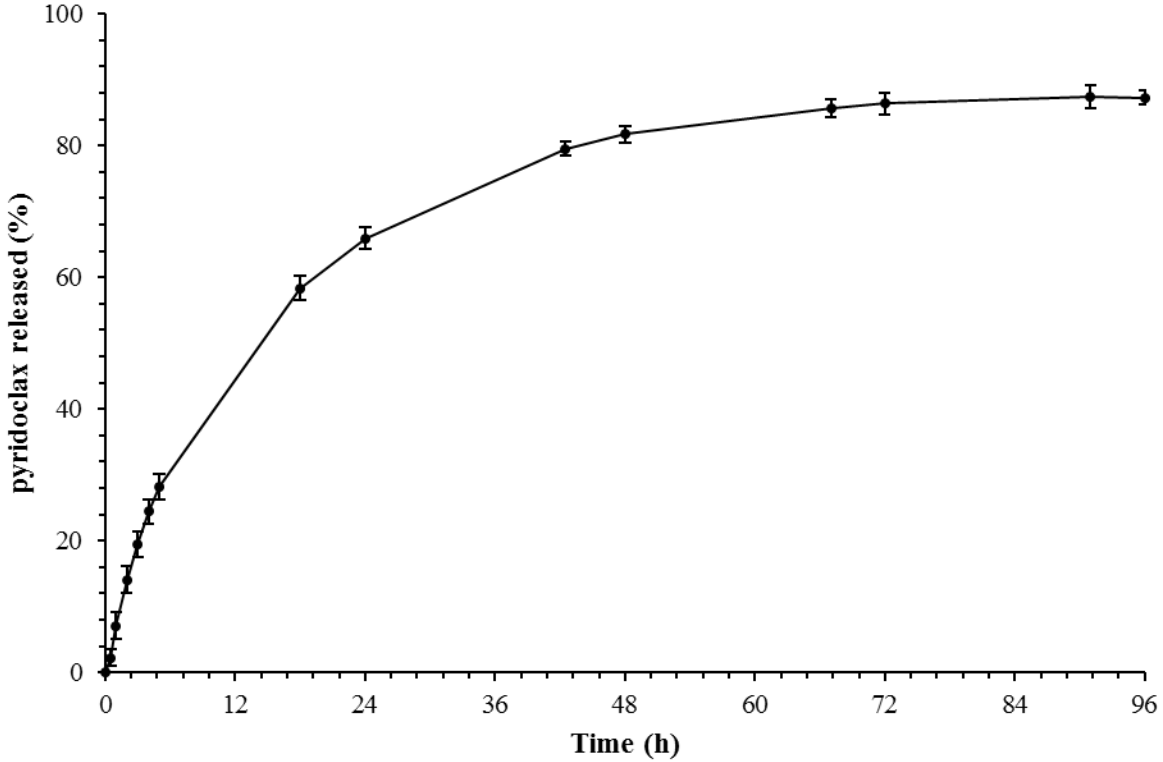

Figure 2. Pyridoclax release kinetics in sink conditions of 2 wt% drug loaded nanoemulsions (Mean ± standard deviation (n=3))

Figure 3. Effect of Pyridoclax and PNEs on IGROV1-R10 ovarian cancer cells, alone or associated with a Bcl-x_L targeting drug (ABT-737). Cellular morphology was studied by phase contrast microscopy (left panel), nuclear morphology after DAPI staining (center panel), and DNA content histograms by flow cytometry (right panel).

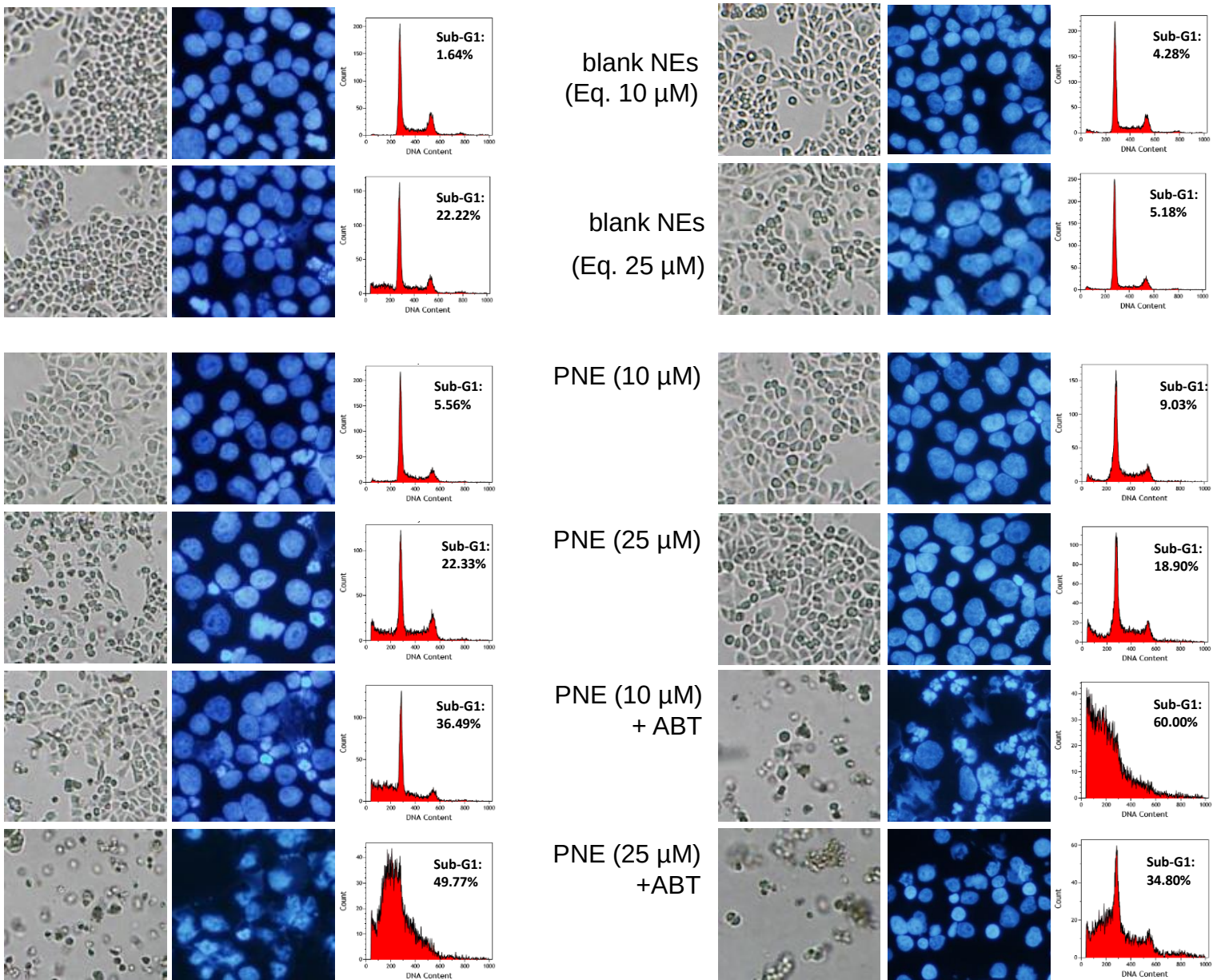

Figure 4. Effects of increasing concentrations of Pyridoclax and PNEs as single agent or associated with a Bcl-x_L targeting drug (5 µM ABT-737) on IGROV1-R10 ovarian cancer cells. Real time cellular activity was assessed by imaging of caspase 3/7 activation.

A

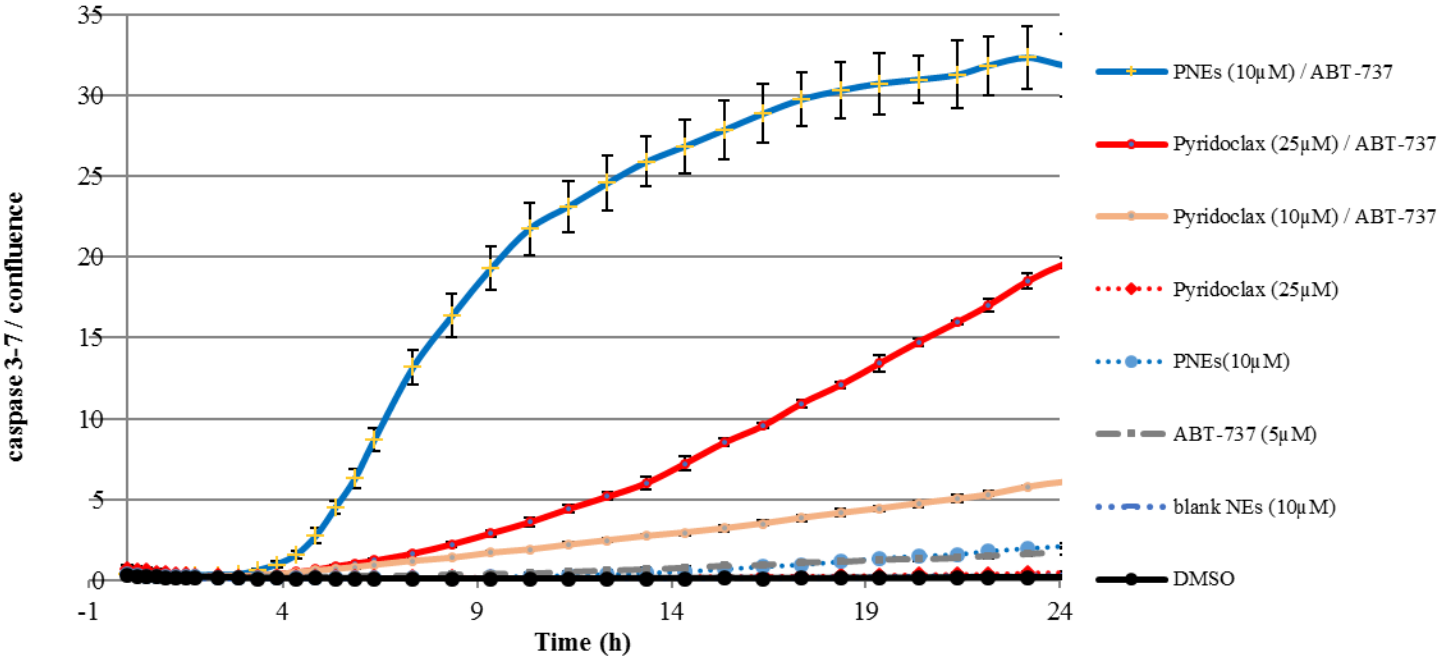

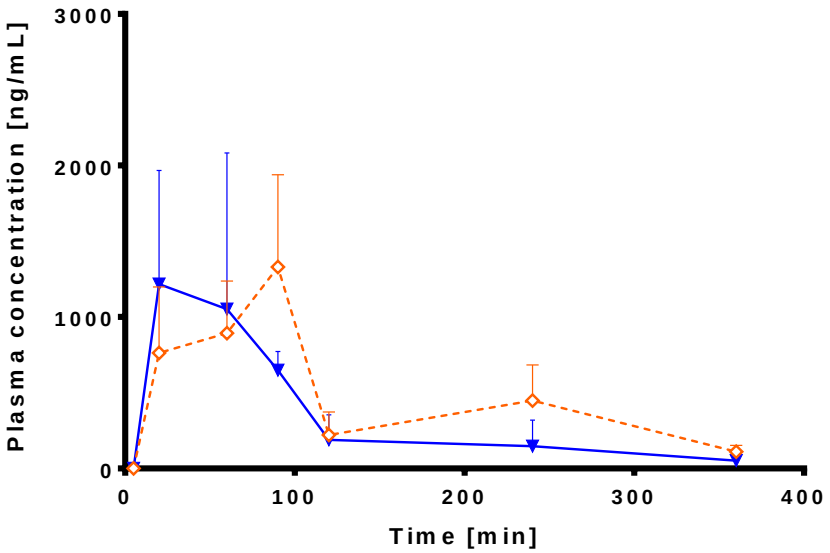

Figure 5. Plasma Pyridoclax concentration–time profiles after the oral administration of a 10 mg/kg dose of Pyridoclax to mice. Full blue triangles: PNEs; empty orange diamonds: Pyridoclax suspension. Each point represents mean ± standard deviation (n=3).

Table 1. UHPLC-MS/MS data used for the quantification and the confirmation of Pyridoclax and internal standard (IS: MR29071)

Compound	Retention time (min)	MRM precursor (m/z)	MRM product ion (m/z)	Collision energy (V)
Pyridoclax	5.99	427.2	349.1 (269.0)	-37 (-50)
IS (MR29071)	5.82	413.1	335.1 (308.1)	-39 (-47)

Table 2. Physico-chemical properties of the studied nanoemulsions, with EE : encapsulation efficiency , DL : drug loading

Formulation	Diameter (nm)	PDI	Zeta potential (mV)	Concentration (mg/mL)	EE (%)	DL(%)
Blank NEs	91.0 ± 3.4	0.155 ± 0.018	-8.1 ± 0.4			
PNEs	105.8 ± 5.1	0.114 ± 0.012	-3.8 ± 1.5	4.2 ± 0.3	96.2 ± 4.7	2.1 ± 0.2

Table 3. Values of the correlation coefficients (r^2) and drug release rate constant (K) obtained by fitting Pyridoclax release data from the nanoemulsions with zero order, first order and square of time release mathematical models

zero order		**first order**		**√t**	
r^2	K ($mg.h^{-1}$)	r^2	K (h^{-1})	r^2	K ($mg.h^{-1/2}$)
0.9409	0.0192	0.6047	0.098	0.9895	0.1055

Table 4. Pharmacokinetic parameters after oral administration of Pyridoclax suspension (Pyr-Susp), and Pyridoclax-loaded nanoemulsions (PNEs). Mean ± standard deviation (n=3), CI= Confidence Interval

	Pyr-Susp	**PNEs**
C_{max} [ng/mL]	1330 ± 609	1200 ± 751
T_{max} [min]	60	20
$AUC_{(0 \text{ to last})}$ and CI [10^5 ng.min/mL]	1.63 ± 0.22 [1.11; 2.24]	1.16 ± 0.27 [0.45; 2.07]
$AUC_{(0 \text{ to inf})}$ and CI [10^5 ng.min/mL]	1.83 ± 0.22 [1.26; 2.40]	1.21 ± 0.27 [0.50; 2.09]
MTT (Mean Transit Time) and CI [min]	182.2 ± 25.8 [144.2; 257.4]	118.1 ± 23.6 [65.5; 194]

Pyridoclax, a new Mcl-1 inhibitor

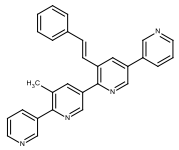

versus

Pyridoclax-loaded nanoemulsions

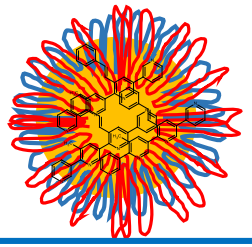

Activity on resistant ovarian cancer cells, associated with a Bcl-x_L targeting drug (ABT-737)

Free Pyridoclax + ABT

10µM

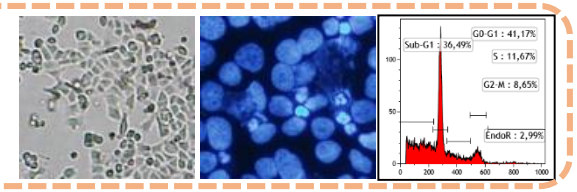

25µM

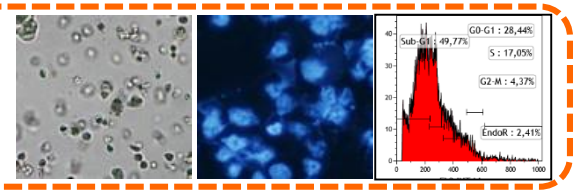

Pyridoclax-loaded NEs + ABT

10µM

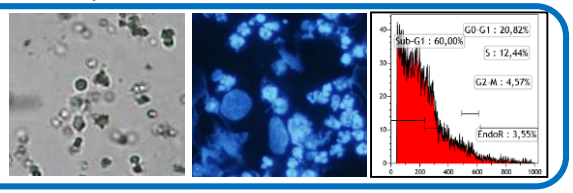

Imaging of real time caspase 3/7 activation

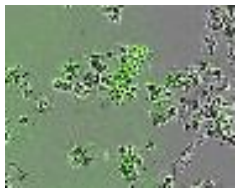

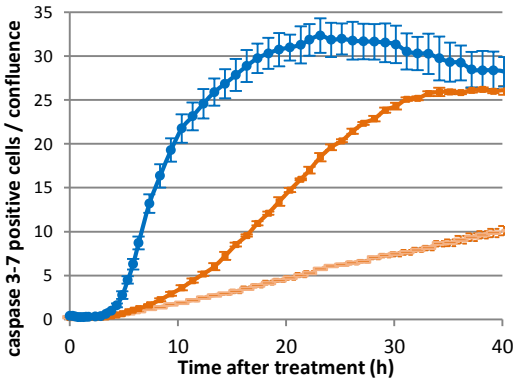

Pharmacokinetics after oral administration on mice